

Photodissociation of formic acid

Hongmei Su, Yong He, and Fanao Kong^{a)}

Institute of Chemistry, Chinese Academy of Sciences, Beijing, 100080 People's Republic of China

Weihai Fang and Ruozhuang Liu

Department of Chemistry, Beijing Normal University, Beijing, 100875 People's Republic of China

(Received 10 November 1999; accepted 28 February 2000)

The photodissociation of formic acid has been studied experimentally and theoretically. *Ab initio* calculations were performed to study the dissociative profiles of five reaction channels on the S_0 , S_1 , and T_1 potential energy surfaces. The vibrationally excited nascent products were detected using a time-resolved Fourier transform infrared spectrometer after laser photolysis at 248 or 193 nm. In the 248 nm photolysis, the HCOOH molecule was first excited to the S_1 state, but it was found that the dissociation takes place on the S_0 surface after internal conversion. The products of the vibrationally excited CO, $\text{CO}_2(v_3)$ and $\text{H}_2\text{O}(v_1)$ were detected. During the dissociation process the vibrationally energized molecule is geometrically memorized and dynamically controlled, with the yield preference of CO and H_2O over that of CO_2 and H_2 . The ratio of $\text{CO}(v \geq 1)/\text{CO}_2(v \geq 1)$ is estimated as <7.5 . Vibrationally excited CO (v) and $\text{CO}_2(v_3)$ are also found in the 193 nm photolysis but the CO/ CO_2 ratio increases to 11. Most of the dissociation is thought to occur on the S_0 state. At this wavelength another dissociation channel which produces OH and HCO radicals on S_1 surface has been identified. The dissociation is unlikely to occur on the T_1 surface, as the energy barriers are fairly high. © 2000 American Institute of Physics. [S0021-9606(00)00620-6]

I. INTRODUCTION

As the simplest carboxylic acid, formic acid is an important intermediate in the oxidation of unsaturated hydrocarbons in combustion.¹ HCOOH is also the ultimate intermediate of the reaction $\text{CH}_2 + \text{O}_2$. Decomposition of formic acid leads to the end products CO and CO_2 in flames.² It is also the simplest interstellar molecule containing a carboxyl group, which has been identified in the interstellar cloud Sgr B₂.^{3,4}

The ground state S_0 (X^1A') of HCOOH is of C_s symmetry with a planar geometry. The first absorption $S_1 \leftarrow S_0$ refers to $\pi^* \leftarrow n$ transition of the carbonyl group.⁵ Sugarman reported that the absorption spectrum consists of diffuse bands from 250 to 225 nm, which merge into continuum below 225 nm.⁶ This diffusion spectrum reflects the predissociative behavior of HCOOH in the excited state. Ng *et al.* have reported a weak absorption at the wavelengths greater than 260 nm.⁷ This band became progressively sharper at longer wavelength.

The five dissociation channels that can possibly occur in the photolysis of formic acid are given in Table I.

The table also lists the available energy ($E_{\text{avail}} = h\nu - \Delta H_o^\circ$) after photolysis at 248 and 193 nm.

Thermal decomposition of the ground-state S_0 has been experimentally and theoretically investigated by several groups.⁸⁻¹¹ All of these studies agree that in the pyrolysis of HCOOH the most important reactions are via "molecular elimination" in reactions (1) and (2). Channel (1) was found to be the predominant reaction. Early *ab initio* computations

indicated that the energy barrier (81.6 kcal/mol) of channel (1) is higher than that (62.1 kcal/mol) of channel (2), while recent theoretical calculations^{12,13} indicate that the two barriers have similar heights, 68 kcal/mol for channel (1) and 71 kcal/mol for channel (2).

Channels (3)–(5) can only occur from electronically excited states because of the higher energy requirement for these reactions. Singleton *et al.*¹⁴⁻²⁰ carried out a series of photolysis experiments at 222 nm, detecting the photolysis products by the laser induced fluorescence (LIF) method. For the OH product, a quantum yield of 0.70–0.80 was determined.¹⁴⁻¹⁹ So they suggested that the photolysis of the S_1 state is dominated by channel (3). In addition, they observed a small amount of CO and CO_2 by static Fourier-transform infrared (FTIR) spectroscopy.²⁰ However, they could not distinguish whether these two products were generated directly from channels (1) and (2) or indirectly via channels (4) and (5). By LIF spectroscopy, Ebata²¹ *et al.* observed OH fragment from the photolysis of HCOOH at several wavelengths between 250 and 220 nm. Almost no vibrational excitation ($f_v \leq 0.009$) and very low rotational excitation ($f_r \leq 0.06$) were found for the OH product. They proposed that channel (3) might take place in the S_1 state with a nonplanar structure. On the other hand, predissociation through an internal conversion to the S_0 state was also possible. Brouard *et al.*²² recorded the LIF and resonantly enhanced multiphoton ionization (REMPI) spectra for OH and HCO radicals, respectively, after the photolysis of HCOOH at 225 nm. They discussed the character of the transition state and suggested that channel (3) occurred via predissociation from the S_1 state.

^{a)} Author to whom correspondence should be addressed; electronic mail: kong@mrdlab.icas.ac.cn

TABLE I. The five dissociation channels that can possibly occur in the photolysis of formic acid.

		ΔH° (kcal/mol)	$E_{\text{avail}}(248 \text{ nm})$ (kcal/mol)	$E_{\text{avail}}(193 \text{ nm})$ (kcal/mol)
HCOOH \rightarrow CO+H ₂ O	(1)	6.3	108.7	140.7
\rightarrow CO ₂ +H ₂	(2)	-3.5	118.5	150.5
\rightarrow HCO+OH	(3)	96.8	18.2	50.2
\rightarrow HCOO+H	(4)	106.1	8.9	40.9
\rightarrow H+COOH	(5)	91.1	23.9	55.9

The previous investigations of the photolysis of HCOOH suggest that the photolysis mechanism is still obscure. In this paper, we report our experimental results on the dissociation of formic acid at 193 and 248 nm. We also report theoretical calculation of the dissociation profiles from the S_0 , S_1 , and T_1 potential energy surfaces (PES). The equilibrium geometries, intermediate structures, and energy barriers, as well as product states are found. Experimental investigations of the laser photolysis of formic acid used time-resolved Fourier transform infrared (TR FTIR) spectroscopy to follow vibrationally excited products. Nascent products were found and thus the preferable dissociation channels have been determined. Furthermore, the reaction mechanisms on the S_0 , S_1 , and T_1 surfaces have been discussed based on the theoretical calculations and the experimental results.

II. EXPERIMENT

The experiment was performed with a TR FTIR apparatus which uses laser photolysis to produce vibrationally excited products. The details of the setup and the TR FTIR spectrometer have been described elsewhere.²³ Briefly, an excimer laser beam at 248 nm (KrF laser, Lambda Physik LPX305i, ≈ 150 mJ/pulse) or 193 nm (ArF laser, Lambda Physik LPX305i, ≈ 60 mJ/pulse) was slightly focused into the reaction chamber by a cylinder lens ($f=380$ nm). The photolysis chamber was pumped by a diffusion pump. The HCOOH (98%) vapor flowed into the reaction chamber with the pressures of 10, 30, 60, and 130 Pa, respectively. The infrared (IR) emissions from photofragments were collected by a pair of gold-coated spherical mirrors and directed into a FTIR spectrometer (Nicolet 800). An InSb detector was used to detect the IR emission. The spectral resolution of the instrument was set at 16 cm^{-1} . Ten time-sequenced interferograms with a spaced $18 \mu\text{s}$ after the laser pulse could be acquired with a data acquisition system.

There exists an equilibrium between the monomer and the dimer of HCOOH²⁴ with equilibrium constant $K_{\text{eq}}=[\text{HCOOH}]^2/[\text{HCOOH}]_2=1.09\times 10^{-7} \text{ mol/cm}^{-7}$. The concentrations of monomer at different vapor pressures are presented in Table II. At all of the pressures the IR emissions after laser photolysis were observed.

III. COMPUTATIONAL DETAILS

Ab initio calculations are used to explore the ground-state S_0 for internal rotation, decarboxylation, and dehydra-

TABLE II. Concentration of monomer at different formic acid vapor pressure.

Vapor pressure (Pa)	Concentration of monomer (%)
10	95.5
30	91.5
60	84.3
130	73.9

tion reactions of formic acid. The geometry optimization, vibrational frequency, and IRC calculations are carried out at the MP2 level using 6-311G(*d,p*).

The stationary structures on the lowest triplet T_1 and the first excited singlet S_1 surfaces were fully optimized with the complete active space self-consistent field (CASSCF) method without any symmetry constraints. Once convergence was reached, the harmonic frequencies were examined, so that true minima or saddle points could be confirmed. In the CASSCF calculations, the active space consists of seven orbitals which originate from the π , π^* , and n orbitals of the carboxylic group and the C-H, O-H, or C-O σ and σ^* orbitals, providing eight electrons. The energy of the separating fragments was determined by a supermolecular calculation with the same basis set and active space as that in the calculations of the bound fragments. The correlation-consistent atomic natural orbital basis sets, cc-pVDZ and cc-pVTZ,²⁵ were employed. The geometry of

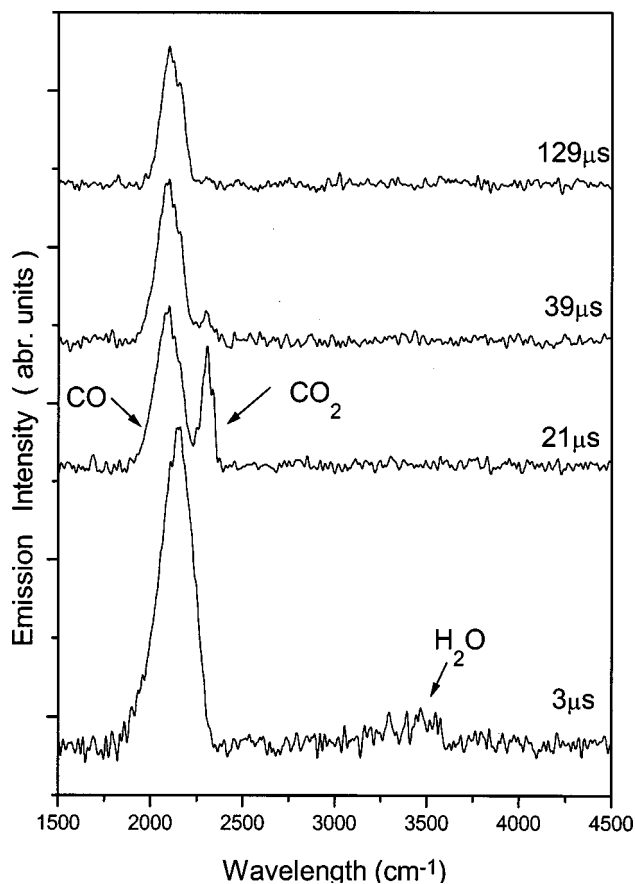


FIG. 1. The infrared emission spectra of HCOOH ($P_{\text{HCOOH}}=60$ Pa) photolyzed by a 248 nm laser at different delay time.

HCOOH (S_0) is also optimized at the CAS(8.7)/cc-pVDZ and CAS(8.7)/cc-pVTZ levels in order to obtain the relative energies of the stationary points on the excited-states' surfaces. The CAS (8.7)/cc-pVDZ zero-point vibrational energy was scaled by a factor of 0.85 in calculations of the barrier heights and reaction energies. All the *ab initio* calculations have been performed with the GAUSSIAN 94 or G98W program packages.²⁶

IV. RESULTS AND DISCUSSIONS

A. Photolysis at 248 nm

1. Products

Three IR emission bands were recorded when formic acid was photolyzed by the 248 nm laser. Figure 1 shows emission spectra at different delay times after laser firing. In the 3 μ s spectrum an intense emission between 1820 and 2370 cm^{-1} was recorded, representing an overlap of CO and CO₂(ν_3) emission bands. The hot products are relaxed mainly by collisional quenching. The overlapping band splits into two components 18 μ s later in the second spectrum. The 1820 to 2220 cm^{-1} components are assigned to the $v \rightarrow v - 1$ emission of CO, while the other between 2220 and 2390 cm^{-1} is attributed to the ν_3 mode of the $v \rightarrow v - 1$ emission of CO₂. The CO₂(ν_3) emission decays very fast and almost disappears at 39 μ s after the laser pulse. Such rapid vibrational relaxation can be interpreted as near-resonant $v - v$ energy transfer from the hot CO₂(ν_3) to the precursor molecule HCOOH (C=O stretching mode, 2325 cm^{-1}). In contrast, the relaxation of CO(v) is slower. A fairly intense emission of CO($v \rightarrow v - 1$) can still be observed at 129 μ s.

In the 3 μ s spectrum, another weak emission was recorded between 3125 and 3625 cm^{-1} . It might be assigned to the ν_1 mode of the H₂O molecule generated from channel (1) or to OH from channel (3). Due to only a small amount of available energy (~ 18 Kcal/mol) in channel (3), it was difficult to vibrationally excite the OH product. Ebata²¹ also reported that there is almost no vibrational excitation of the OH radical generated in photolysis. Therefore, this emission band is assigned to the ν_1 mode of H₂O.

2. Spectral simulation

The contour line of the CO and CO₂ emission spectra has been simulated. The IR emission intensity of each rovibrational transition has been normalized by the corresponding Einstein spontaneous emission coefficient $A(v, J)$. Therefore, the relative population of each rovibrational state of the CO and CO₂ molecules is obtained. At a pressure of 60 Pa, more than ten collisions take place between the molecules in 3 μ s. The rotational excitation has been substantially quenched by this time. We therefore used a specific rotational temperature T_R to represent the rotational population. The best fitted T_R at 3 μ s for CO and CO₂ are 450 and 550 K, respectively, while a T_R of 350 K is suitable to fit the spectra after 21 μ s. Figure 2 shows a comparison between the experimental and simulated spectra at 3 μ s.

As the vibrational quenching is relatively inefficient, the vibrational population at 3 μ s delay is still close to that of the nascent products. Table III presents the relative vibra-

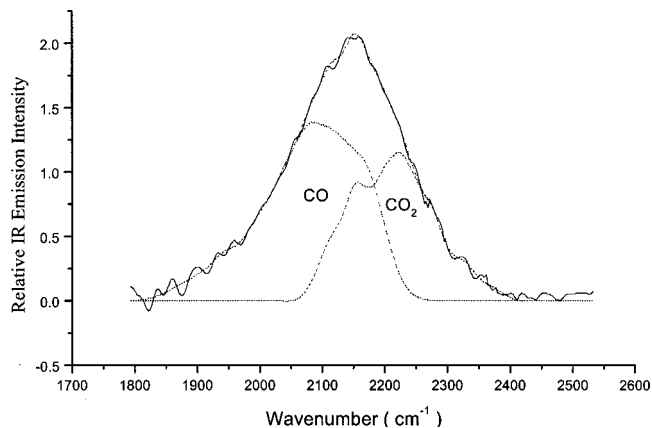


FIG. 2. The experimental and simulated infrared emission spectra of CO and CO₂(ν_3) at 3 μ s after 248 nm laser shots. The simulated individual emission band of CO and CO₂ at 3 μ s is also given by the dashed lines.

tional populations at 3 μ s after the photolysis. Both the CO and CO₂ products are highly vibrationally excited. There is an apparent population inversion for CO₂. The most populated level is $v = 5$. At the longer delay times, the emission band of CO₂ shifts toward higher frequency due to vibrational relaxation (Fig. 2).

The yield ratio of the CO($v > 0$) and CO₂($\nu_3, v > 0$) is 30, which is estimated by comparing their total populations listed in Table III. The populations have been normalized by the Einstein A coefficients; the sum of the populations reflects the relative concentrations of the excited CO($v > 0$) and CO₂($\nu_3, v > 0$) molecules. Each CO₂ molecule has three vibrational modes (ν_1 , ν_2 , and ν_3) with a double degeneracy of ν_2 . We can only record the ν_3 mode by the InSb detector used in the experiment. Assuming the vibrational energy is individually and equally distributed among all three modes, the total population of the CO₂ might be four times than that of the CO₂(ν_3) mode. The yield ratio of CO/CO₂ at 3 μ s delay then roughly equals CO/4CO₂(ν_3), or 7.5. As the vibrational quenching of CO₂ is much faster than that of CO, it is anticipated that the yield ratio CO/CO₂ of the nascent products must be less than 7.5. Furthermore, the above ratio refers only to the vibrationally excited CO and CO₂ species. The ground state ($v = 0$) is not included, although it might be not important.

3. Channel identification

The nascent products of CO, CO₂, and H₂O are directly observed in the spectrum. Yield dependence of CO and CO₂ on laser power was measured to be 1.0 ± 0.1 and thus the two-photon process is ruled out. Both products are highly vibrationally excited. They should be generated from a highly exothermic channel. For single-photon photolysis at 248 nm, the large amount of the available energy, 109 kcal/mol released from channel (1) or 119 kcal/mol from channel (2), is sufficient to excite CO or CO₂(ν_3) up to $v = 11$. All of this indicates that the photolysis pathways are through channels (1) and (2).

TABLE III. Relative vibrational population of CO and CO₂ at 3 μ s (HCOOH photolyzed by 248 and 193 nm, $P_{\text{HCOOH}}=60$ Pa).

		$v=1$	$v=2$	$v=3$	$v=4$	$v=5$	$v=6$	$v=7$	$v=8$	$v=9$	$v=10$	$v=11$	Total	Ratio (CO/CO ₂)
248 nm	CO	22.97	16.98	9.08	4.77	2.46	1.43	1.75	1.15	0.87	0.41	0.20	62.07	7.5
248 nm	CO ₂	0.16	0.21	0.16	0.14	0.30	0.26	0.28	0.18	0.11	0.21	0.05	2.06	
193 nm	CO	12.00	3.44	3.35	1.06	1.18	1.05						22.08	11
193 nm	CO ₂	0.06	0.17	0.28									0.51	

B. Photolysis at 193 nm

1. Products

The 193 nm photolysis of HCOOH was accomplished by using an ArF laser. Figure 3 shows the IR emission spectra of the photofragments. In the 3 μ s spectrum, three emission bands were recorded. Again, the emissions between 1960 and 2360 cm^{-1} are attributed to the overlapping bands of CO (v) and CO₂(ν_3), similar to the one at 248 nm.

A new emission centered at 1864 cm^{-1} was also observed. It is assigned to the C–O stretching mode of HCO (fundamental vibrational frequency being 1868 cm^{-1}). The H₂O(ν_1) emissions were not observed, perhaps because of the low signal-to-noise ratio in the spectrum.

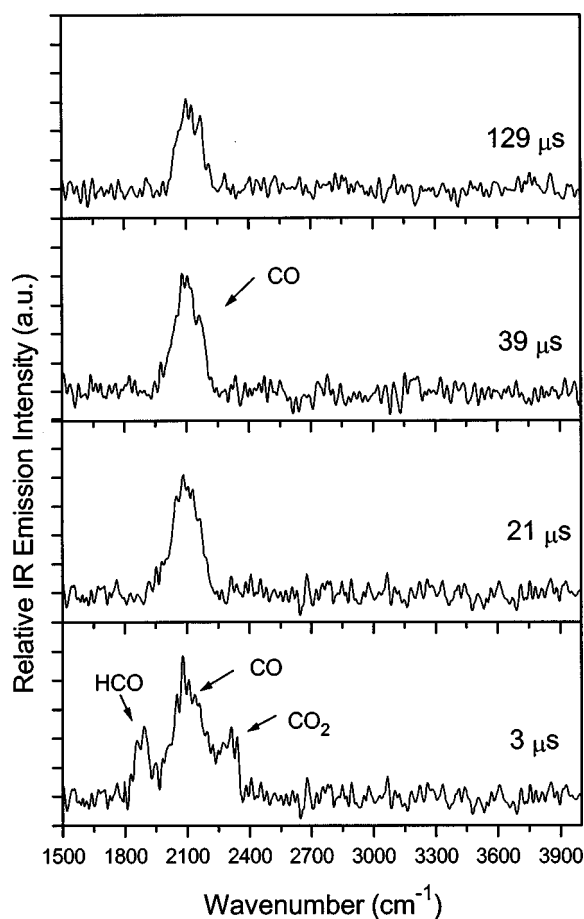


FIG. 3. The infrared emission spectra of HCOOH ($P_{\text{HCOOH}}=60$ Pa) photolyzed by a 193 nm laser at different delay time.

2. Vibrational populations

Spectral simulations were also performed for the emission spectra of CO(v) and CO₂(ν_3) at the delay of 3 μ s. The vibrational populations were presented in Table III. Comparison between the simulated and experimental spectra is shown in Fig. 4. The highest vibrational energy levels populated in CO and CO₂ are at $v=6$ and $v=4$, respectively, which are slightly lower than those in the 248 nm photodissociation.

A ratio of the excited CO(v) to CO₂(ν_3, v) is obtained as 44 by comparing the total populations, and the yield ratio of 11 is estimated for the CO($v>0$)/CO₂($v>0$) with the same assumption in the above analysis of 248 nm photolysis.

3. Channel identification

The observation of highly vibrationally excited products CO and CO₂ again verifies the occurrence of channels (1) and (2). The CO(v)/CO₂(ν_3) ratio of 11 indicates that the channel (1) is a more important pathway. However, channel (3) has been identified by the observation of the HCO(ν_2).

C. The dissociative profiles of the potential energy surfaces

1. S₀ state

The geometries of *cis*- and *trans*-formic acid in the S₀ state are optimized at the CASSCF and MP2 levels with cc-pVDZ, cc-pVTZ, and 6-311G(*d,p*) basis sets (Fig. 5). The barriers of the isomerization from the *trans*- to the *cis*-

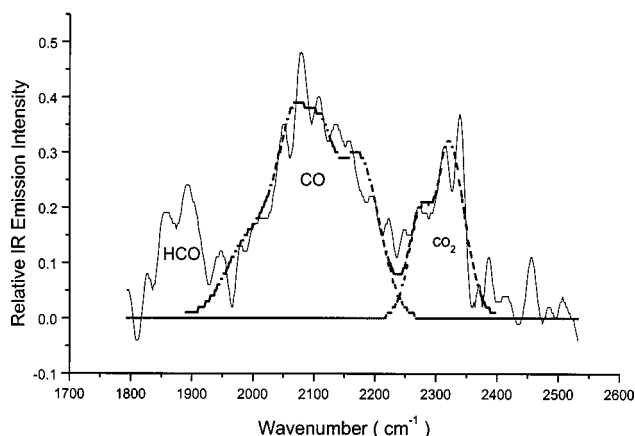


FIG. 4. The experimental and simulated infrared emission spectra of CO and CO₂(ν_3) at 3 μ s after 193 nm laser shots. The simulated individual emission band of CO and CO₂ at 3 μ s is also given by the dashed lines.

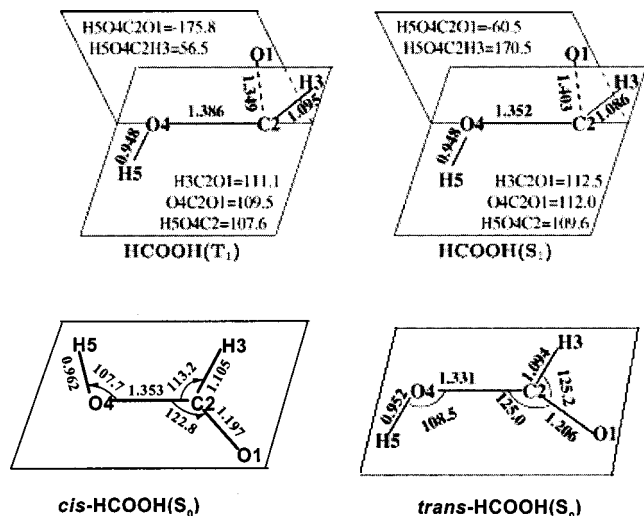


FIG. 5. The geometric structures of the minima in the S_0 , T_1 , and S_1 surfaces (bond length in Å; bond and dihedral angles in degree).

isomer are calculated to be 12.5 kcal/mol at the MP2/6-311G(*d,p*) level. This value is in agreement with previous result of 13 kcal/mol.¹² The *cis*- and *trans*-isomers link to the products of H_2+CO_2 and H_2O+CO , respectively, with solid lines in the energy correlation diagram (Fig. 6). For the reaction channel (1), our calculated barrier height from the *trans*-isomer is 67.6 kcal/mol, agreeing with Goddard's result of 68 kcal/mol.¹² Our calculated barrier of channel (2) is 67 kcal/mol, which is lower than the Goddard's result of 71 kcal/mol.

The S_0 surface can also be accessible to the radical channels (3)–(5) shown by the solid lines in Fig. 6. No transition state was found in the reaction pathways. The potential energy profiles correlate to the products with the energy of 102.1, 93.0, and 112.5 kcal/mol higher, respectively.

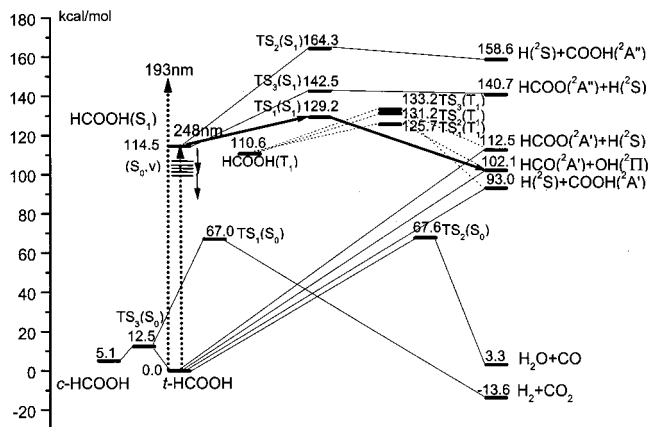


FIG. 6. The dissociative profiles of S_0 , S_1 , and T_1 surfaces in the photodissociation of HCOOH. The data are calculated at the MP2 and CAS(8,7) level using the 6-311G(*d,p*), cc-pVDZ, and cc-pVTZ level. The solid lines link singlet surfaces while the dashed lines correlate the states in the T_1 surface.

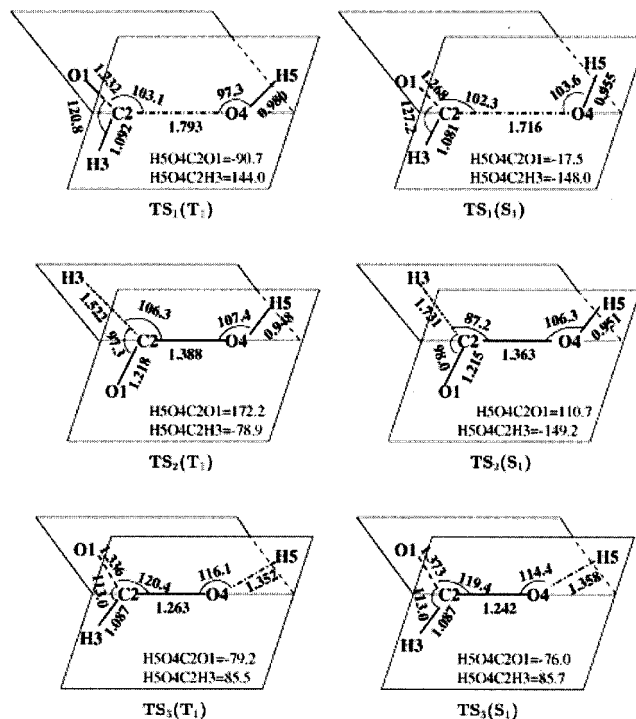


FIG. 7. The geometric structures of the saddle points in the T_1 and S_1 surfaces (bond length in Å; bond and dihedral angles in degrees).

2. S_1 state

The S_1 minimum at the CAS (8,7) level with the cc-pVDZ basis set has a nonplanar structure, shown in Fig. 5. The calculated 0-0 energy gap between S_0 and S_1 is 114.5 kcal/mol, which is comparable with the band origin at 38 463 cm^{-1} (110 kcal/mol).^{6,7} There are three possible dissociation pathways on the S_1 surface. The most feasible channel is (3), leading to two ground-state radicals, $OH(^2\Pi)$ and $HCO(^2A')$. There is a transition state $TS_1(S_1)$ with a low energy barrier of 14.7 kcal/mol at the CAS (8,7)/cc-pVDZ level. The geometry of the transition state, $TS_1(S_1)$, is shown in Fig. 7.

The second dissociation pathway on the S_1 surface leads to $H(^2S)$ and $COOH(A^2A'')$ with a high barrier of 49.8 kcal/mol (Fig. 6). The third reaction pathway on the S_1 surface correlates to the $H(^2S)$ and the excited $HCOO(^2A'')$, which is 28.2 kcal/mol above the ground state $HCOO(^2A')$. The optimized geometry of the transition state $TS_3(S_1)$ is also shown in Fig. 7, while the barrier height is calculated as 28.0 kcal/mol.

3. T_1 state

The stationary structure of the T_1 minimum is optimized at the CAS (8,7) and MP2 levels with the cc-pVDZ and cc-pVTZ basis sets. Figure 5 shows the CAS (8,7)/cc-pVDZ nonplanar structure. There are also three dissociation pathways on the T_1 surface. In contrast to the S_1 surface, the T_1 surface is only accessible to the products in their ground states shown by the dashed lines in Fig. 6. For channel (3), a first-order saddle point [$TS_1(T_1)$] is found. $TS_1(T_1)$ is confirmed by the IRC calculations as the transition state, leading to $HCO(^2A')$ and $OH(^2\Pi)$. The barrier height is 15.1 and

14.6 kcal/mol at CAS(8,7)/cc-pVDZ and CAS(8,7)/cc-pVTZ levels, respectively. A scaled CAS(8,7)/cc-pVDZ zero-point energy correction is made for the barriers. The spin contamination in the reference wave function is very small. The expectation value of the S^2 operator is very close to 2.00 for the pure triplet state.

Unlike that in the S_1 surface, the second dissociation pathway in the T_1 surface correlates to the products of $H(^2S)$ and the ground-state $COOH(^2A')$. The latter is 65.6 kcal/mol lower than that of the excited state $COOH(^2A'')$. The corresponding energy barrier (20.6 kcal/mol) is also lower than that on the S_1 surface (49.8 kcal/mol).

The third pathway on the T_1 surface leads to the fragments of $H(^2S)$ and the ground-state $HCOO(^2A')$. A barrier height of 22.6 kcal/mol is calculated.

D. Reaction mechanism

1. 248 nm photolysis

The diffuse bands between 250 and 225 nm in the absorption spectrum indicate that HCOOH undergoes predissociation. Energetically, a 248 nm photon (115 kcal/mol) can barely excite a HCOOH molecule from the S_0 to the S_1 state (114.5 kcal/mol). Obviously, the excited molecule is unable to undergo the dissociation reactions (3)–(5) either on the S_1 or on the T_1 surfaces. However, an internal conversion of $S_1 \rightarrow S_0$ followed by decomposition of the molecule on the S_0 surface is possible. In the 248 nm experiment, the dissociation products are CO_2 , CO, and H_2O . The observation also supports that molecular elimination takes place in the S_0 state, just like in the pyrolysis of HCOOH. Again, the above mechanism is supported by the energy disposal in the products. Goddard *et al.* predicted that the CO_2 produced in the S_0 state should be highly vibrationally excited.¹² Our population analysis (Table III) shows that the CO and CO_2 products of 248 nm are indeed vibrationally hot.

The CO/ CO_2 ratio of 7.5 shows that channel (1) is dominant, although the energy barriers of channels (1) and (2) are the same on the S_0 surface, but the preference of the reactions can be explained by their dynamic behavior. Because the lifetime of the highly vibrational excited HCOOH molecule is very short, there is not enough time to statistically redistribute the energy over various vibrational modes. The fate of the highly energized molecule is dynamically controlled. The preference of forming $CO+H_2O$ over CO_2+H_2 may be due to geometric feature of the transient species. As shown in Fig. 7, the two H atoms are located on the opposite sides of the O–C–O plane in the S_1 minima. The H_2 -eliminating reaction could not take place with this geometry. In contrast, the geometry is feasible to channel (1), which produces $CO+H_2O$, simply via a H atom hopping process.

2. 193 nm photolysis

Absorbing a 193 nm photon, formic acid (S_0) can be excited to the high vibrational levels of the S_1 state. The wavelength of 193 nm is in the continuum region of the absorption spectrum. Therefore, a strongly dissociative feature of the highly energized molecule is anticipated. The ex-

cess energy (148–114.5=33.5 kcal/mol) is sufficient to overcome the low barrier (14.7 kcal/mol) of channel (3), producing HCO and OH radicals (Fig. 6). The HCO was observed in this experiment and the OH was recorded by other groups.^{14–19}

The CO and CO_2 in the 193 nm photolysis arise from the decomposition of the highly vibrationally excited S_0 state HCOOH after an internal conversion of $S_1 \rightarrow S_0$. The ratio of the nascent CO/ CO_2 molecules is higher than that in the 248 nm case, suggesting that the formation mechanisms at the two wavelengths are similar. Furthermore, we assume that the most energized S_1 molecule is consumed with the reaction channel (3). Only the remaining less energetic molecule converts to the S_0 state. Therefore, the highest vibrational levels of the $CO(v)$ and $CO_2(v)$ found in the 193 nm photolysis are lower than 248 nm ones.

Dissociation on the T_1 surface is not likely to occur, because there is a series of fairly high energy barriers that must be overcome. The barriers for forming $H+COOH$ and $H+HCOO$ are calculated as 20.6 and 22.6 kcal/mol, respectively. The COOH and HCOO formed are unstable. Further decomposition has been well studied by Schatz *et al.*^{27–29} The most favorable dissociation pathway of HCOO is forming $H+CO_2$ with a barrier of 16.3 kcal/mol. The COOH dissociates to $OH+CO$ through a loose transition state at 35.6 kcal/mol. In addition, the requirement of 35.6 kcal/mol in the latter pathway would cause a relatively minor production of CO compared to that of CO_2 . However, our observation of the CO/ CO_2 ratio showed the opposite results. Therefore, the CO and CO_2 are probably not produced on the T_1 surface. Furthermore, CAS(8,7)/cc-pVDZ calculations indicate that both S_1 and T_1 have similar ($n-\pi^*$) electronic configuration. It is well known that the spin-orbit coupling is small.³⁰ Therefore, it is likely that the direct intersystem crossing from S_1 to T_1 is not efficient.

V. CONCLUDING REMARKS

- (1) Five dissociation channels of formic acid are theoretically studied. *Ab initio* calculations were performed on the ground-state S_0 and the excited states S_1 and T_1 surfaces. The optimized geometries, energy minima, transition states, and energy barriers along the dissociative profiles of the PES are found.
- (2) The photodissociation of formic acid was studied at 248 and 193 nm wavelengths, respectively. The nascent photofragments were detected by TR FTIR spectroscopy.
- (3) After the photolysis of HCOOH, vibrationally excited fragments of $CO(v \leq 8)$, $CO_2(v_3, v \leq 9)$, and $H_2O(v_3)$ at 248 nm, and $CO(v \leq 6)$, $CO_2(v \leq 5)$, and $HCO(v_2)$ at 193 nm were observed. The vibrational excitation of CO and CO_2 is slightly lower at 193 than that at 248 nm.
- (4) The photolysis of HCOOH at 248 nm occurs primarily via the two molecule-elimination channels of $HCOOH \rightarrow CO+H_2O$ and $HCOOH \rightarrow CO_2+H_2$. The branching ratio of the two channels is estimated as <7.5 . The mechanism is believed to be a dissociation process in the S_0 state after an internal conversion from S_1 to S_0 .
- (5) A new product, i.e., HCO, is observed in 193 nm photolysis. This product is probably formed on the S_1 sur-

face. But CO and CO₂ are formed on the S₀ surface. The CO(*v*)/CO₂(*v*₃,*v*) ratio is 11, which indicates that the dissociation mechanism is analogous to the 248 nm case.

- (6) The high CO/CO₂ yield ratio can be explained on the basis of dynamic and geometric reasons. The energized, *trans*-like HCOOH molecule suddenly dissociates, preferably producing H₂O+CO before the vibrational energy can be statistically redistributed in the molecule.

ACKNOWLEDGMENTS

The work is supported by the China National Science Foundation under Contract Nos. 29873008 and 29773052, and by China DOST. The authors are also grateful to Professor Q. Zhu for helpful discussion.

- ¹W. C. Gardiner, Jr., *Combustion Chemistry* (Springer-Verlag, Berlin, 1984), p. 294.
²H. M. Su and F. Kong, *Chem. Phys. Lett.* **322**, 21 (2000).
³B. Zuckerman *et al.*, *Astrophys. J. Lett.* **163**, L41 (1971).
⁴G. Winnewisser and E. Churchwell, *Astrophys. J. Lett.* **200**, L33 (1975).
⁵J. G. Calvert and J. N. Pitts, Jr., *Photochemistry* (Wiley, New York, 1966), p. 428.
⁶B. Sugarman, *Proc. Phys. Soc. London* **55**, 429 (1943).
⁷T. L. Ng and S. Bell, *J. Mol. Spectrosc.* **50**, 166 (1974).
⁸P. G. Blake, H. H. Davis, and G. E. Jackson, *J. Chem. Soc. B* 1971 (1923).
⁹D. S. Y. Hsu, W. M. Shaub, M. Blackburn, and M. C. Lin, *The Nineteenth International Symposium on Combustion* (The Combustion Institute, Pittsburgh, 1983), p. 89.
¹⁰M. C. Lin and K. J. Laidler, *Trans. Faraday Soc.* **64**, 94 (1968).
¹¹K. Saito, T. Kakumoto, H. Kuroda, S. Torri, and A. Imamura, *J. Chem. Phys.* **80**, 4989 (1984).
¹²J. D. Goddard, Y. Yamaguchi, and H. F. Schaefer III, *J. Chem. Phys.* **96**, 1158 (1992).
¹³J. S. Francisco, *J. Chem. Phys.* **96**, 1167 (1992).
¹⁴G. S. Jolly, D. J. McKenney, D. L. Singleton, G. Paraskevopoulos, and A. R. Bosard, *J. Phys. Chem.* **90**, 6557 (1986).

- ¹⁵D. L. Singleton, G. Paraskevopoulos, R. S. Irwin, G. S. Jolly, and D. J. McKenney, *J. Am. Chem. Soc.* **110**, 7786 (1988).
¹⁶D. L. Singleton, G. Paraskevopoulos, and R. S. Irwin, *J. Am. Chem. Soc.* **111**, 5248 (1989).
¹⁷G. S. Jolly, D. L. Singleton, D. J. McKenney, and G. Paraskevopoulos, *J. Chem. Phys.* **84**, 6662 (1986).
¹⁸G. S. Jolly, D. L. Singleton, and G. Paraskevopoulos, *J. Phys. Chem.* **91**, 3463 (1987).
¹⁹D. L. Singleton, G. Paraskevopoulos, and R. S. Irwin, *J. Phys. Chem.* **94**, 695 (1990).
²⁰R. S. Irwin, D. L. Singleton, G. Paraskevopoulos, and R. McLaren, *Int. J. Chem. Kinet.* **26**, 219 (1994).
²¹T. Ebata, T. Amano, and M. Ito, *J. Chem. Phys.* **90**, 112 (1989).
²²M. Brouard, J. P. Simons, and J. X. Wang, *Faraday Discuss. Chem. Soc.* **91**, 63 (1991).
²³Q. Zhu, S. Huang, X. Wang *et al.*, *Chinese J. Chem. Phys.* **6**, 87 (1993).
²⁴J. O. Halford, *J. Chem. Phys.* **15**, 111 (1947).
²⁵T. H. Tunning, Jr., *J. Chem. Phys.* **90**, 1007 (1989).
²⁶GAUSSIAN 98 (Revision A.3), M. J. Frisch, G. W. Trucks, H. B. Schlegel, G. E. Scuseria, M. A. Robb, J. R. Cheeseman, V. G. Zakrzewski, J. A. Montgomery, R. E. Stratmann, J. C. Burant, S. Dapprich, J. M. Millam, A. D. Daniels, K. N. Kudin, M. C. Strain, O. Farkas, J. Tomasi, V. Barone, M. Cossi, R. Cammi, B. Mennucci, C. Promelli, C. Adamo, S. Clifford, J. Ochterski, G. A. Petersson, P. Y. Ayala, Q. Cui, K. Morokuma, D. K. Malick, A. D. Rabuck, K. Raghavachari, J. B. Foresman, J. Cioslowski, J. V. Ortiz, B. B. Stefanov, G. Liu, A. Liashenko, P. Piskorz, I. Komaromi, R. Gomperts, R. L. Martin, D. J. Fox, T. Keith, M. A. Al-Laham, C. Y. Peng, A. Nanayakkara, C. Gonzalez, M. Challacombe, P. M. W. Gill, B. G. Johnson, W. Chen, M. W. Wong, J. L. Andres, M. Head-Gordon, E. S. Replogle, J. A. Pople, Gaussian, Inc. Pittsburgh, PA, 1998.
²⁷G. C. Schatz, M. S. Fitzcharles, and L. B. Harding, *Faraday Discuss. Chem. Soc.* **84**, 359 (1987).
²⁸K. Kudla, G. C. Schatz, and A. F. Wagner, *J. Chem. Phys.* **95**, 1635 (1991).
²⁹K. S. Bradley and G. C. Schatz, *J. Chem. Phys.* **106**, 8464 (1997).
³⁰N. J. Turro, *Modern Molecular Photochemistry* (University Science, Mill Valley, CA, 1991).